Synthesis and characterization of novel eco-epoxy adhesives based on the modified tannic acid for self-healing joints

Nataša Z. Tomić [a],[*], Milad Saeedifar [b], Mohamed Nasr Saleh [b],[d],[**], Aleksandar Marinković [c], Dimitrios Zarouchas [b], Sofia Teixeira de Freitas [b]

[a] *Innovation Center of Faculty of Technology and Metallurgy in Belgrade Ltd, Karnegijeva 4, Belgrade, Serbia*
[b] *Structural Integrity & Composites Group, Faculty of Aerospace Engineering, Delft University of Technology, the Netherlands*
[c] *Faculty of Technology and Metallurgy, University of Belgrade, Karnegijeva 4, 11070, Belgrade, Serbia*
[d] *Advanced Materials Research Center, Technology Innovation Institute, Masdar City, Abu Dhabi, United Arab Emirates*

ARTICLE INFO

ABSTRACT

The aim of this research was to investigate the self-healing potential of damaged Al joints when bonded using novel eco-epoxide adhesives derived from tannic acid (TA). Two eco-epoxy components based on TA, (A) glycidyl ether and (B) glycidyl phosphate ester of TA, were produced. The effect of the eco-epoxy components on the self-healing ability was assessed in terms of the energy dissipation recovery after partial failure in a double cantilever beam (DCB) test, which was compared to the reference epoxy (R). The self-healing process required 2 h and 2 bars in an autoclave at 180 °C. Techniques such as DSC, FTIR and DMA showed residual activity and potential self-healing capability of the used adhesives. A combination of two monitoring techniques, Digital Image Correlation (DIC) and Acoustic Emission (AE), was used to monitor the strain distribution and damage propagation in the DCB specimens. The healing index for adhesives R, B and A was found to be 8.9%, 3.0%, and 82.5% respectively. The findings of this work highlighted the potential of using bio-based epoxy adhesives in structural adhesive bonding, as well as the prospect of utilizing their self-healing ability to restore the strength of such bonded parts.

1. Introduction

Polymers, nowadays, are commonly used in different industries such as transportation, electronics, stationery, sports equipment, and civil engineering [1]. Mechanical, thermal, chemical, ultraviolet radiation, and other causes, on the other hand, may cause deep microcracks in the structure, resulting in deformation or destruction. During the service life of such polymeric components, traditional repair techniques fail in restoring unseen microcracks within the system. In the 1980s, the idea of self-healing polymeric materials was proposed to patch invisible microcracks and prolong the stability and service life of polymerized parts [2]. Self-healing polymer materials, in principle, have the potential to significantly recover their load transfer capability after being impaired. This type of recovery can occur naturally or as a result of the application of a particular treatment (such as radiation, heat, and water). As a result, these products are expected to greatly increase the reliability and protection of polymeric parts while mitigating the need

for expensive active inspection or external servicing [3]. Therefore, there has been a growing need for self-repairing materials. Until now, the majority of the obtained self-healing materials are petroleum-based, and available literature is limited mostly to their healing properties [4–6]. However, as fuel resources become limited and the climate is adversely affected, scientists' attention has shifted to green and environmentally sustainable biomass products. Redundant bio-sources like sodium alginate, proteins, chitosan, cellulose, and natural rubber have also been used in the development of polymer materials [7]. A bio-based material is a material that is produced from ingredients obtained from living (or previously living) organisms. So far, the self-healing mechanism of bio-based polymers can be classified into two categories: i) the use of healing agents [8–10], and ii) intrinsic healing through the reversible chemical bonds [11–13].

The repair method is one of the most pressing problems in the field of adhesively bonded joints. Although adhesive bonding offers the highest load transfer and structural performance, adhesives have mostly been

---

confined to secondary structures due to concerns regarding the bonded joints' fatigue and longevity throughout their structural lifespan [14], as well as the difficulties of testing a bond line after manufacturing and in-service [15]. Both issues could be solved by introducing self-healing adhesives with a longer lifespan and reduced maintenance costs. Very few studies dealt with self-healing epoxy adhesives in the bonding of structural materials such as steel and aluminum (Al) [16,17]. The majority of these research studies are based on the microencapsulation technique, which is usually toxic, expensive, and time-consuming.

Thus, the aim of this study is to investigate the self-healing capability of fractured Al joints bonded with novel eco-epoxide adhesives synthesized from a bio-renewable raw material (tannic acid – TA). This paper proposes a new repair method of adhesively bonded joints using the intrinsic healing capability of TA. In order to support the mechanical macroscopic response with detailed analysis and provide a better understanding of the phenomenon, non-destructive testing (NDT) methods such as acoustic emission (AE) and digital image correlation (DIC) are utilized. Proving the high healing efficiency of such bio-based adhesives in the bonding of lightweight structures can raise the level of confidence and importance of using bio-based adhesives in structural bonding.

2. Materials and manufacturing

2.1. Adhesives and adherends

Chemicals used in the synthesis of the modified TA: sodium hydroxide (NaOH), epichlorohydrin (EPH), N-methyl-2-pyrrolidone (NMP), phosphorus oxychloride (POCl₃), deionized water (MiliQ), chloroform, magnesium sulfate, Tetrahydrofuran (THF), glycidol, and calcium chloride were used as received from Sigma Aldrich, USA. The solvent used for the surface cleaning, acetone, was supplied by Sigma Aldrich, USA. The reference adhesive was selected to be BPA-based epoxy (LG700 epoxy component and HG 700R curing agent). It was supplied by GI-NI ltd, Belgrade, Serbia (epoxy value 0.62, $T_g = 79.4$ °C). The adherend selected was Al alloy 2024.

2.2. Modification of tannic acid

2.2.1. Synthesis of glycidyl ether of TA
The reaction of TA with EPH at 80 °C and a 1:1.5 wt ratio of TA to 20% NaOH solution in methanol yielded glycidyl ether of TA (or saturated water solution) [18]. EPH (15 g) was dissolved in THF (15 mL) for 30 min at room temperature with magnetic stirring. The solution was then transferred to a 100 mL three-neck round-bottomed flask fitted with a reflux condenser, pressure-equalizing dropping funnel, nitrogen intake tube, and the TA (3 g) was added before heating to 80 °C with magnetic stirring. Then, using a dropping funnel, 22.5 mL 20% NaOH solution (4.5 g NaOH in 18 mL water) was added dropwise while stirring. To complete the process, the system was heated up to 80 °C for 3 h. The solution was then cooled down before being gradually added to 200 mL cold MiliQ water. After extracting the product with toluene (3 × 70 mL), the organic extract was dried overnight with MgSO₄. To maintain a high vacuum, the toluene solution was transferred to a flask equipped with a short distillation column, Liebig condenser, and receiver (app. 1000 Pa). To eliminate all volatile remaining chemicals in TA's glycidyl ether, a simultaneous increase in temperature (2 °C/min) was followed by a drop in pressure. The obtained product was highly viscous brownish oil. The observed epoxy equivalent weight (EEW) was 170 g/mol, implying that 10 epoxy groups were inserted per TA molecule. In a previously published paper, the chemical structure was described and analyzed [19].

2.2.2. Synthesis of glycidyl phosphate ester of TA
The glycidyl phosphate ester of TA was made using a newly established process for making fire retardant epoxy components [20]. TA (6 g) was introduced to a 250 mL three-neck round-bottomed flask fitted

with vacuum distillation equipment and two pressure-equalizing dropping funnels. Then, it was dissolved at room temperature in 50 mL of a 1:1 ratio combination of chloroform and NMP. The temperature of the oil bath was set to 70 °C after 30 min. The first dropping funnel was loaded with a 9.75 g POCl₃ solution in 20 mL chloroform, while the second was loaded with 9.42 g glycidol dissolved in 40 mL chloroform. The reaction was started by dropwise addition of POCl₃ solution under continual stirring and low vacuum (1 kPa) as soon as the temperature reached 70 °C. After 10 min, glycidol was added dropwise for the following 2 min. The addition was repeated in a 1:2 ratio, and once all of the chloroform had been added, the temperature was adjusted to 85 °C with the vacuum steadily increased until all of the chloroform had been removed. When the vacuum was raised to eliminate NMP, the reaction proceeded for 12 h (vacuum at 10 Pa). When the reaction was accomplished, the product was purified in the same way that the glycidyl ether of TA was purified. The obtained product was highly viscous light brown oil. The observed epoxy equivalent weight (EEW) was 85 g/mol, implying that 20 epoxy groups were inserted per TA molecule via 10 phosphoryl linkages. In a previously published paper, the chemical structure was described and analyzed [19].

The chemical structure of both types of adhesive components, obtained by modification of TA, is presented in Fig. 1.

2.3. Surface pretreatments and bonding

Prior to bonding, the surface preparation of aluminum samples was as follows: step I – acetone cleaning, step II - grit blasting with Al₂O₃ powder (Corublast Super Z-EW No. 40, Ø 0.35–0.50 mm), step III – acetone cleaning and step IV – air blow duster gun.

Three adhesives were selected for testing the adhesion on the Al adherend: 1) reference epoxy adhesive (R); 2) epoxy adhesive with 15 wt% of modified tannic acid with epichlorohydrin (adhesive A); and 3) epoxy adhesive with 15 wt% of modified tannic acid with phosphoryl chloride and glycidol (adhesive B). Glass bead spacers (150–250 μm), used for adhesion thickness control, were mixed with the adhesives at 0.1 wt% prior to bonding. Fig. 2 shows the schematic representation of the sample preparation and panel dimensions. Bonding of Al panels was performed at room temperature, left to cure for 24 h, with post-curing at 70 °C for 4 h. After curing, the samples were machined to 25 mm width each.

3. Experimental procedure

The experimental campaign was carefully designed to be able to tackle all the important aspects and meet the objectives of this research study. The DSC analysis represents the first step in this systematic approach to determine: i) whether or not the synthesized adhesives can react from a chemical point of view indicating their self-healing potential and ii) if this is true, what the healing process parameters: temperature and duration, should be. This was followed by the FTIR analysis, which provided sufficient information about the structural changes after the healing process and what these changes could imply. Finally, the DMA analysis was very important to investigate/quantify the effect of such changes, captured by the FTIR, on the mechanical properties of the bulk adhesive; in other words, to determine how these changes are reflected from a mechanical point of view. Despite the knowledge obtained from this systematic approach, this is still not a complete understanding because these techniques are not capable of capturing the changes at the interface level, which is the scope of this research study. Thus, it was very important to test the self-healing hypothesis using some common interface characterization techniques such as mode I Double Cantilever Beam (DCB) testing. Besides, in-situ monitoring techniques such as DIC and AE were utilized to confirm and capture the changes between the virgin and healed specimens, if any, during the DCB testing. The subsections below detail each of the techniques used in the aforementioned proposed order.
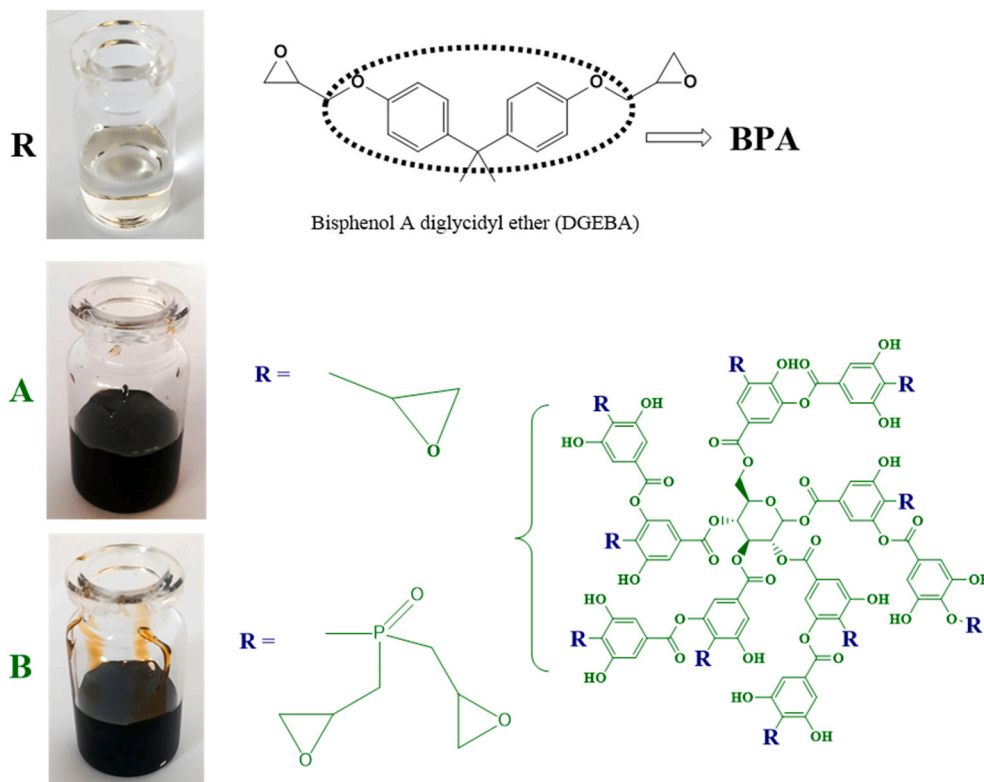
Fig. 1. Schematic representation of used adhesives and the type of tannic acid modification.
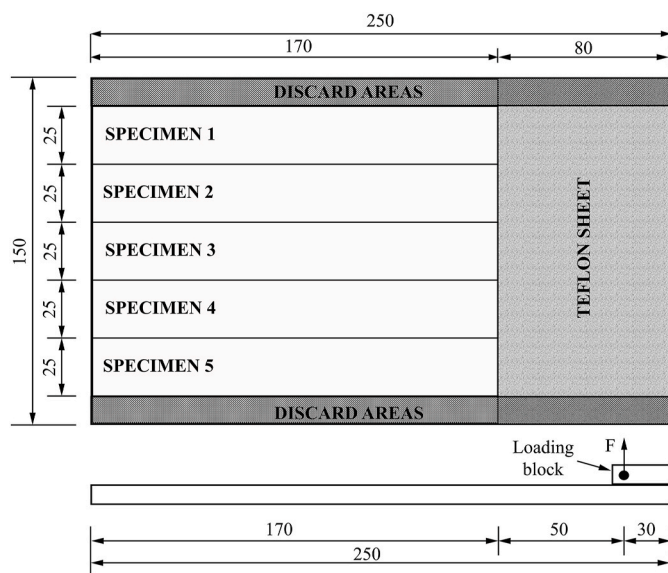

Fig. 2. Schematic representation of sample preparation.

3.1. Physical and chemical characterization

3.1.1. DSC analysis

Differential scanning calorimetry (DSC) is a method for measuring heat flows and temperatures associated with the material thermal transitions. The DSC analysis can be used to assess a variety of material properties, including glass transition temperatures, melting and crystallization cases, phase transitions, cure kinetics, and oxidation and other chemical reactions. The used epoxy adhesives and bio-based components were tested by the DSC technique to investigate the self-healing capability and healing temperature. DSC analysis was performed on DSC250, TA Instruments, in a temperature range of 20–200 °C, using N_2 atmosphere.

3.1.2. FTIR analysis

FTIR spectroscopy of epoxy components used in adhesive preparation was performed to confirm the obtained structure of the synthesized components and to compare the presence of functional groups that can affect the bonding interface. Analysis was done using a Nicolet™ iS™10 6700 spectrometer (Thermo Scientific) in the attenuated total reflectance (ATR) mode with a single bounce 45 °F Golden Gate ATR accessory with a diamond crystal, and DTGS detector. FTIR spectra were obtained at 4 cm^{-1} resolution with ATR correction. The FTIR spectrometer was equipped with OMNIC software and recorded the spectra in the wavelength range from 2.5 μm to 20 μm (i.e., 4000 –500 cm^{-1}).

3.1.3. DMA analysis

Dynamic mechanical analysis (DMA) is an important extension of thermal analysis because it can show fine temperature transitions that influence the material's complex modulus. The visco-elastic analysis of the used epoxy adhesives was performed by Perkin Elmer Diamond DMA RSA-G2 in a tension fixture (rectangle), at the temperature range 25–200 °C, and angular frequency 6.28319 rad/s.

3.2. Double cantilever beam (DCB) testing

The mode I fracture toughness DCB test was carried out, according to the ISO 25217 standard [21], using the displacement-controlled mode, with a displacement rate of 3 mm/min. The machine used for testing was a Zwick Roell machine equipped with a 10 kN load cell and hydraulic grips to minimize the slippage due to gripping. The machine recorded both the crosshead displacement and the applied force during the test. The test setup is depicted in Fig. 3 a. DCB test was monitored by combined in-situ monitoring techniques DIC and AE, which are indicated in Fig. 3 b. All the specimens had the same nominal dimensions (length × width ~ 250 mm × 25 mm) with a 70 mm long Teflon sheet to act as the
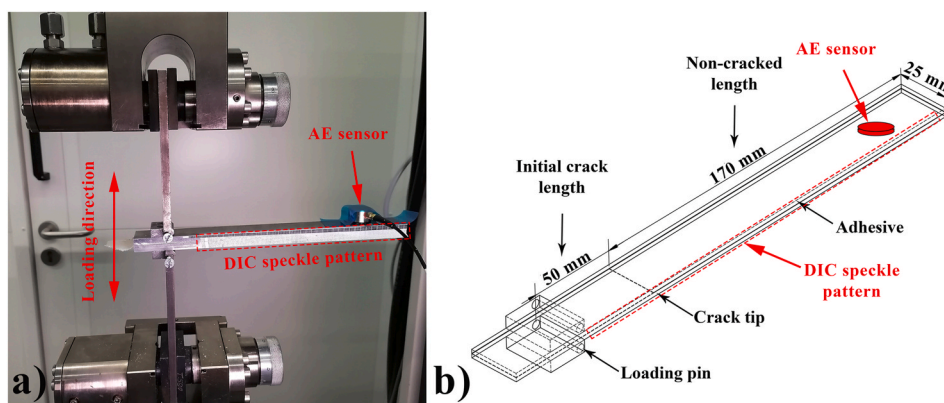
Fig. 3. a) DCB test setup and b) schematic of the DCB specimen.

crack initiator (see Fig. 2). All specimens were designed so that the distance between the loading pin and the initial crack tip is ~50 mm as per the ISO 25217 standard procedure. The only difference was the adherends' thickness being 6 mm. For each adhesive type, three specimens were tested to ensure the reproducibility and repeatability of the results.

After the destructive mechanical tests of the virgin samples, the samples were re-joined at elevated temperatures. However, it is important to highlight that the test was stopped before reaching complete separation of the DCB specimen to be able to evaluate the efficiency of the healing approach. The test procedure was repeated in order to evaluate the self-healing capability of novel bio-based adhesives.

3.3. In-situ monitoring techniques

3.3.1. Digital image correlation (DIC)

In order to visualize the strain contour map ahead of the crack tip [22,23] and measure the crack length throughout the test [24], a two-dimensional (2D) DIC system (see Fig. 3 a) was used. The DIC system consisted of one 8-bit "Point Grey" camera with a resolution of 5 MP, equipped with a "XENOPLAN 1.4/23" lens. The software used for capturing and recording the speckle pattern images was ViC-Snap 8, a product of "Correlated Solutions Inc.". The acquisition rate of 1 and 0.33 frames per second (fps) was used for the initial and reloading tests respectively. Afterward, the acquired images by ViC-Snap 8 were processed using ViC-2D 2009 software. For processing, the subset size was set to 20 × 20 pixels with a step size (distance between subsets) of 5 pixels. The observation window of approximately (650 × 650) mm^2 produced an image with dimensions of (2048 × 2048) pixels.

3.3.2. Acoustic emission (AE)

In order to record the produced AE signals during the DCB test, one AE sensor was placed on the top Al surface of the specimen (see Fig. 3 b). The AE sensor was broadband, resonant-type, and single-crystal piezo-electric transducer from Vallen Systeme GmbH, AE1045SVS900 M, with an external 34 dB pre-amplifier and an operating frequency range of [100–900 kHz]. An AMSY-6 Vallen, 8-channel AE system with a sampling rate of 2 MHz, was used to record the AE signals. Ultrasound gel was applied between the surfaces of the sensor and the specimen to ensure good acoustical coupling. The AE threshold was set as 40 dB.

3.4. Self-healing procedure

Tested samples from DCB (partially fractured) were subjected to self-healing treatment at 180 °C and pressure of 2 bars (1 from the vacuum and 1 of pressure) in a Scholtz Autoclave. The heating temperature rate was 3 °C/min, the dwell time was 2 h, and the cooling rate was 3 °C/min.

3.5. Surface characterization

Post-mortem fractured surfaces of representative samples from each tested group were analyzed using a 3D optical microscope with a wide-area 3D measurement system, type VR-5200 from Keyence, USA.

4. Results and discussion

4.1. Physical characterization

4.1.1. DSC analysis

DSC characterization was performed to investigate the self-healing capability of the used adhesives and the structural changes that occurred during the self-healing treatment. As samples didn't have previous thermal history, since they were cast, cured, and tested directly, Fig. 4 shows the DSC results obtained in the two runs for all the tested adhesives R, A and B. In the first run, adhesive R had the lowest glass transition temperature (T_g) of all the tested adhesives, i.e. 63 °C (Fig. 4 a). Both A and B adhesives had $T_g = 70$ °C (Fig. 4 b and 4c) in the first run. A higher value of T_g for A and B, in comparison with R, was a result of the higher restriction of the polymer chain rotation motions due to the higher reactivity and larger amount of available epoxy groups leading to higher cross-linking density [25]. The first run also showed the exothermic reaction for all samples with a peak temperature of ~175 °C. The exothermic reaction corresponded to the high-temperature curing, i.e. homopolymerization of residual epoxy groups, which remained due to the intentional usage of a lower amount of hardener to improve the self-healing capability of the system. The onset temperature of this exothermic peak was R – 107 °C, A – 119 °C and B – 129 °C. The difference in the onset temperature was affected by the T_g, i.e. the extent of the restriction of the polymer chain movement, which was necessary for the polymerization reaction to take place. The reason for the higher value for B compared to A is the fact that molecule B is larger/bulkier and it also established a higher amount of hydrogen bonding. Hydrogen bonds act like anchors between polymer chains, restricting their movement and delaying the onset of exothermic reaction [26]. The highest enthalpy was observed for adhesive A (9.65 J/g) when compared to B (4.95 J/g) and R (7.64 J/g). The higher the enthalpy, the higher the number of the formed chemical bonds. Thus, adhesive A showed the highest reactivity at high temperatures when compared to R and B. Fig. 5 depicts the possible hypothetical self-healing reactions of adhesives R, A and B at high temperatures. In addition to homopolymerization of epoxy groups (adhesive R), the reaction between the phenolic groups of TA and epoxy can occur as well (A and B) [27]. From the schematic, it can be observed that both the remaining phenolic groups of TA and hydroxyl groups of DGEBA in A are accessible, while the access to phenolic groups of B is sterically hindered by the glycidyl phosphate functional groups. Besides the steric
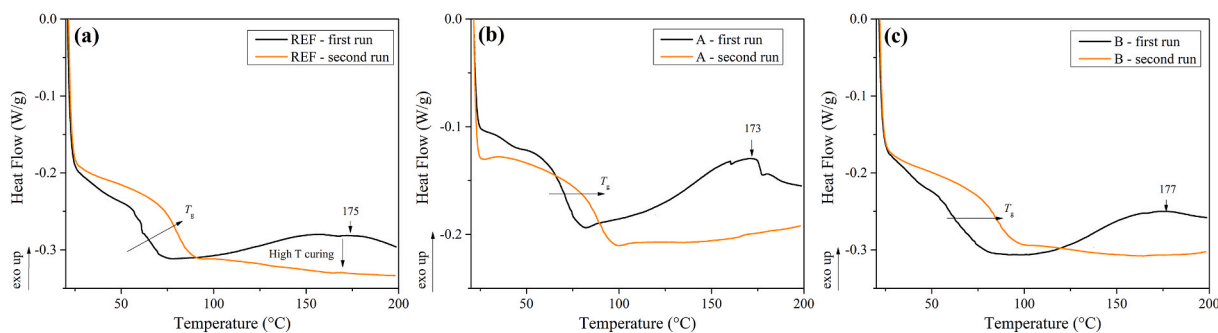
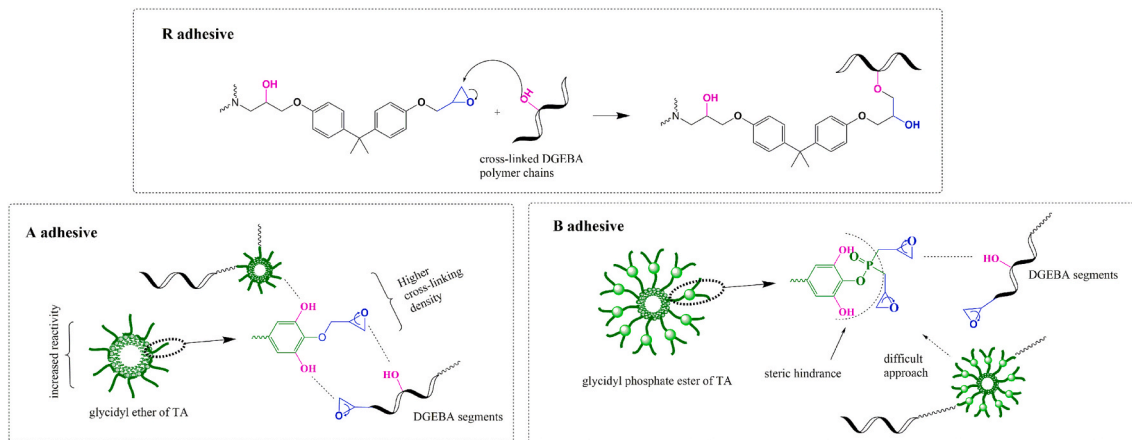**Fig. 4.** DSC analysis of adhesives: (a) R, (b) A and (c) B.

Fig. 5. Possible hypothetical self-healing reactions of adhesives R, A and B at high temperatures.

hindrance, the mobility of bulky molecules of modified TA in cured adhesive B is much lower than in A, making self-healing much difficult to happen. These phenomena in B contributed to the lowest enthalpy of cross-linking of all adhesives. The second DSC run showed that no sample exhibited exothermic reactions after heating up to 200 °C, Fig. 4. All tested adhesives showed an increase in T_g for about ~16 °C, having values of T_g (R) = 79.11 °C (Fig. 4 a), T_g (A) = 87.78 °C (Fig. 4 b) and T_g (B) = 85.18 °C (Fig. 4 c).

All these DSC observations suggested the potential self-healing behavior of adhesive A enabled by the modified tannic acid at higher temperatures. The majority of the exothermic reactions occurred up to 180 °C. Since the phenolic and aliphatic hydroxyl groups react with residual epoxy groups from 115 to 180 °C [27], the temperature of 180 °C was selected as the temperature of the self-healing process. The DSC testing procedure lasted for about 1h, so it was decided that the safe duration of a self-healing process should be 2 h. Nevertheless, the DSC

analysis indicated a residual reactivity of adhesives at high temperatures and a high potential for adhesive A to heal.

4.1.2. FTIR analysis

The FTIR spectra of the virgin and self-healed samples of adhesives R, A and B are shown in Fig. 6. Fig. 6a shows the spectra of DGEBA resin cured with an isophorone diamine (IPDA) hardener. The broad peak at ~3400 cm^{-1} was attributed to hydroxyl groups (O–H) stretching vibrations. Aromatic C–H stretching vibrations were expected at ~2962 cm^{-1} but they were overlapped with the symmetric and asymmetric vibrations of methyl (CH$_3$) and methylene (CH$_2$) groups observed at 2926 cm^{-1} and 2874 cm^{-1}. The characteristic C=C stretching of a benzene ring, present in bisphenol A of DGEBA, was noticed at 1609 cm^{-1}. The C–H in-plane bending vibrations of CH$_3$, symmetrical and asymmetrical, were located at 1364 cm^{-1} and 1459 cm^{-1}, respectively. The peaks at 1248 cm^{-1} and 1105 cm^{-1} correspond to the C–O
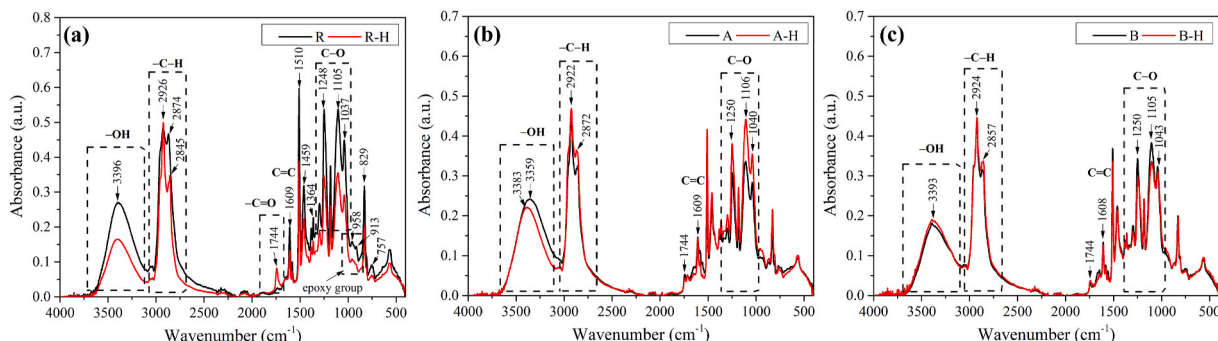

Fig. 6. FTIR spectra of virgin and self-healed samples of adhesives: (a) R, (b) A and (c) B.

stretching vibrations, while the peak at 1037 cm^{-1} originated from C–O stretching in the molecular backbone of the modified epoxy resin containing the anisole-like moiety [28]. The vibration bands at 958, 913, and 757 cm^{-1} correspond to the epoxy groups whose intensity decreases during the curing reactions [29]. The C–N stretching vibration, which corresponds to primary aliphatic amine used as a curing agent in epoxy resin, was observed at 830 cm^{-1} [30].

Characteristic peaks of epoxy resin were observed for adhesives A and B as well, with the difference related to the TA component (Fig. 6b and c). The carbonyl group vibration at 1744 cm^{-1} was noticed for both virgin samples of A and B due to the ester linkages of the TA core [19].

FTIR spectrum of adhesive R after the self-healing process (R–H) showed some structural changes (see Fig. 6a). The main differences were observed regarding the hydroxyl and epoxy group vibration but also the appearance of carbonyl group vibration at 1744 cm^{-1}. A decrease in the amount of both epoxy and –OH groups was expected due to the epoxy resin homopolymerization presented in Fig. 5 for adhesive R. This appearance of the carbonyl group vibration is related to a thermo-oxidation process taking place [31]. In general, the thermo-oxidation process can involve a chain scission and appearance of double bonds, carbonyl, and amide species/moieties, which were reported for the DGEBA/IPDA system [32,33]. Also, the formation of carbonyl groups may occur by the oxidation of secondary hydroxyl groups in cured epoxy resin [34]. This type of oxidation process was followed by a decrease in the intensity of C–O band vibration at 1248 cm^{-1} characteristic for secondary alcohols, which was observed in R–H spectra in Fig. 6a. Two possible pathways of the thermo-oxidation process of DGEBA including the formation of the carbonyl group are presented in Scheme 1.

Judging by the bonds broken and formed, it was noticed that both pathways include the formation of the carbonyl group, which was observed as the appearance of a peak at 1744 cm^{-1} in Fig. 6a. Also, both of them include the breakage of the C–H bond, which is also proved by a decrease of the peak intensity at 2874 cm^{-1} and shifting to a lower wavenumber, i.e. 2845 cm^{-1}. Only the pathway (I) considers the breakage of the O–H bond, which can stand behind some extent of a reduction in peak intensity at 3396 cm^{-1}. The formation of carbonyl groups on the DGEBA backbone was a reason for observed sample yellowing. It has been reported that the yellowing phenomenon occurs for other polymers besides DGEBA due to the mechanism of the carbonyl group formation in the polymer backbone caused by the oxidation process [35,36].

The self-healed process of adhesive A caused structural changes related to decreased O–H and increased C–O peak intensity, Fig. 6b. These changes were in alignment with the presumption of the phenolic groups' involvement in the cross-linking reactions during the self-healing process (see Fig. 5). The absence of the carbonyl group formation in the A-H sample was due to the improved thermal stability and thermo-oxidative resistance by the addition of modified TA [20,37].

FTIR spectrum of the B–H sample showed almost no structural changes after the self-healing process compared to virgin adhesive B (see Fig. 6c). A slight decrease in intensity of C–O stretching vibrations can be attributed to minor rearrangements of C–O groups due to the relaxation

process polymer chains or leaching of oxygen-containing compounds. The most common compound leached in DGEBA epoxy resins was found to be epichlorohydrin [31].

Results from FTIR analysis showed the residual reactivity of the studied adhesives, where the highest was found for R and A, indicating the possible self-healing capability. Besides, the improved thermal stability of adhesives A and B was noticed due to the presence of the modified TA.
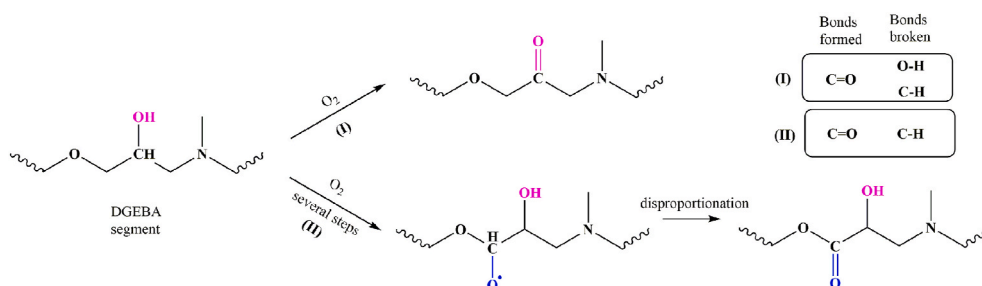
4.1.3. DMA analysis

The chemical composition of the synthesized macromolecules, cross-linking density, the interaction between polymer chains, and TA modification influence on the polymer chains mobility, and phase formation are very important properties of adhesives. Thus, the DMA was used to examine the performance of the novel bio-based adhesives and the effect of the TA component on their properties. Fig. 7 shows the DMA results including the damping factor (tanδ), temperature dependency of the storage modulus (G'), and the loss modulus (G''), which reflects the elastic and viscous behavior of the studied adhesives respectively. The G'_{GS} and G'_{RP} values for glassy state and rubbery plateau, determined at 30 °C and 200 °C respectively, are given in Table 1. The effect of the added TA component on the polymer network structure was investigated by comparing the glass transition temperature (T_g), which was determined as the maximum of tan $\delta(T)$ curve ($T_{g(\tan\delta\ peak)}$). In addition, the height of the peak on the tan$\delta(T)$ curve (tanδ height) and width of the peak on the tan $\delta(T)$ curve (tanδ width), which was determined as the full width at half maximum, was analyzed as well. Values of the cross-linking density (ν) of the adhesives are calculated from the storage modulus in the rubbery state (G'_{RP}) in the following manner [38]:

$$\nu = \frac{G'_{RP}}{RT} \tag{1}$$

where R is the universal gas constant and T (K) = T_g (K)+ 30.

Fig. 7 shows the curves that display samples' transition from the glassy state to the rubbery state or α-relaxation, related to the segmental motion of the polymer chains. Damping factor curves (tan$\delta(T)$) shown in Fig. 7a indicates the glass transition temperature. A significant difference in T_g was observed when compared to the DSC results (see Fig. 4). This difference emphasizes the fact that DMA is more sensitive to transitions in polymers than traditional thermal analysis techniques, such as DSC [39]. For instance, the detection of T_g by DMA is easier in highly filled/reinforced materials because its modulus changes by several orders of magnitudes in the T_g region, while the heat capacity (the basis of T_g detection in DSC) changes less significantly [39]. Besides, DMA is so sensitive that it can recognize weak secondary transitions such as alpha and beta transitions in polymers, which are not masked out by any background noise or other interferences. Nevertheless, there are cases of cross-linked thermosets or heterophase polymers, where the glass transition region is very broad, so neither the peak of the loss modules nor tanδ can give accurate values of T_g [40]. Considering the chemical structures of adhesive R and B (see Fig. 5), it can be said that there is significant heterogeneity in the system of adhesive B compared to R,

Scheme 1. Carbonyl formation reaction involving *i*-propanol moiety on reactive sites of DGEBA [31].
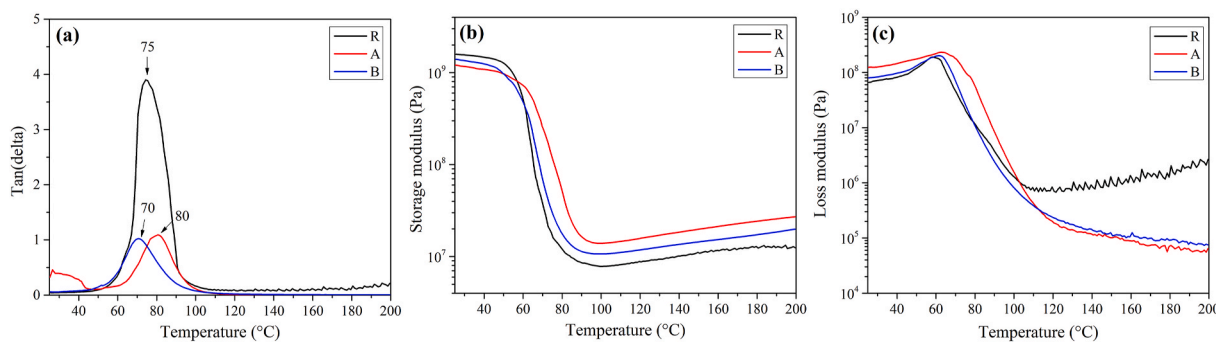
Fig. 7. DMA analysis of tested adhesives R, A and B represented as: (a) tan (delta), (b) storage modulus, G′ and (c) loss modulus, G″

Table 1
Results of DMA analysis of studied adhesives.

Sample	$T_{g\ (tan\delta\ peak)}$ (°C)	$\tan\delta$ height	$\tan\delta$ width [°C]	G'_{GS} (GPa)	G'_{RP} (MPa)	$\nu \cdot 10^3$ (mol/cm³)
R	75	3.90	17.47	1.56	12.49	4.32
A	80	1.09	20.96	1.10	27.12	9.24
B	70	1.02	19.92	1.31	19.89	6.97

which can cause the difference in measuring the T_g by DMA analysis when compared to the DSC. A strong effect of the cross-linking density on the glass transition and the appearance of the $\tan\delta$ curve can be noticed. The low values of damping factor ($\tan\delta$) in $\tan\delta(T)$ curve for adhesives A and B suggested that the formed polymer network had higher cross-linking density than adhesive R [41]. The calculated values of cross-linking density (ν) according to eq. (1) Table 1 shows that adhesive A had more than two times higher ν than adhesive R (114%). Adhesive B had 62% higher ν than adhesive R. When the cross-linking density is higher, the transition loss dispersion decreases in intensity, broadens, and shifts to higher temperatures. Besides, when the cross-linking density is higher, the transition slope of the storage modulus decreases. The improved storage modulus in the rubbery region of adhesives A, when compared to R and B, as a result of the restriction of the free movement of the polymer chains was due to the higher cross-linking density (Table 1) [42]. The loss modulus peak indicated the glass transition, which had lower values of T_g, as expected [40], and still, the highest T_g value for adhesive A. The obtained results from DMA may suggest enhanced mechanical properties of bulk adhesive A due to the highest T_g value and cross-linking density.

4.2. Mechanical characterization and in-situ monitoring

As previously explained in section 3.2, the experimental procedure is designed so that the virgin specimens are tested by propagating the crack length of a_0 to the crack length of a (see Fig. 8), without reaching complete separation. Afterwards, the load is removed to reuse the same specimens for the self-healing investigation. Load-displacement curves for DCB specimens of the three adhesive types at the virgin state are depicted in Fig. 9a. In the virgin state, regardless of the adhesive type, the load-displacement response is characterized by a linear elastic region at the beginning of the loading in which the applied load is correlated to the displacement (Δ) by the stiffness of the aluminum cantilever beam arm. Once the crack-tip opening displacement reaches a critical value, the crack starts to propagate . Comparing the load-displacement curve of the virgin specimens (Fig. 9a) reveals that adhesive B provided the highest maximum load, followed by adhesives R and A respectively. The mode I interlaminar fracture toughness (G_{IC}) of DCB specimens was calculated by the modified cantilever beam theory as follows [21]:
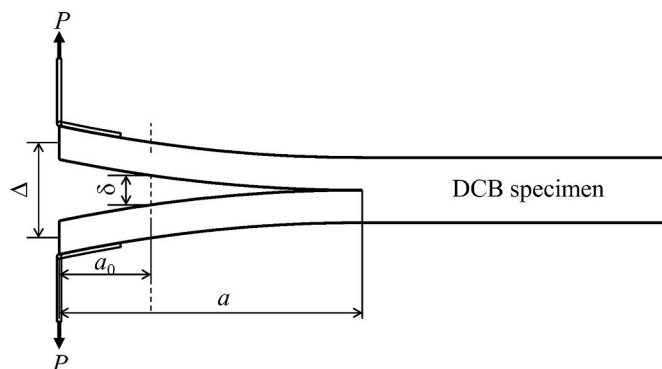

Fig. 8. Schematic representation of the DCB specimen with the initial (a0) and final (a) crack lengths.

$$G_{I-MBT} = \frac{3P\delta}{2b(a + |\Delta|)} \quad (2)$$

where:

P = applied load,
a = crack-length,
b = specimen width,
δ = measured displacement, and
$|\Delta|$ = crack-length correction for a beam that is not perfectly built-in.

The average G_{IC} value of adhesives B, R and A, calculated by Equation (2), is 52.04, 39.40, and 22.65 J/m² respectively. As it is clear, the fracture toughness of adhesive B was more than two times of adhesive A. The higher G_{IC} of adhesive B was referred to the improved adhesion and cohesion by the addition of glycidyl phosphate ester of TA [43], contributing to the improved hydrogen bonding with the adherend. In addition, the modified tannic acid of adhesive B can act as a phosphatizing agent, whose purpose is to improve the adhesion of adhesives, coatings, or paint [44]. In order to achieve this aim, the phosphatizing agent must accomplish two steps: first is to diffuse to the metal interface and achieve good adhesion, and second is to interact with the bulk polymer. These steps are only achieved for virgin samples since the diffusion/penetration of liquid adhesive B was possible but not for the softened adhesive B during the self-healing process at temperatures above the T_g. This phenomenon can further improve both the adhesion and cohesion strength of virgin samples resulting in higher G_{IC} of adhesive B compared to adhesive A. Lower G_{IC} of adhesive A, compared to the adhesive R, was due to the weaker structure, which was expected to be improved after the self-healing process relative to the other two adhesives.

After conducting the mode I test of the virgin DCB specimens, the specimens were cured in the autoclave, according to the procedure
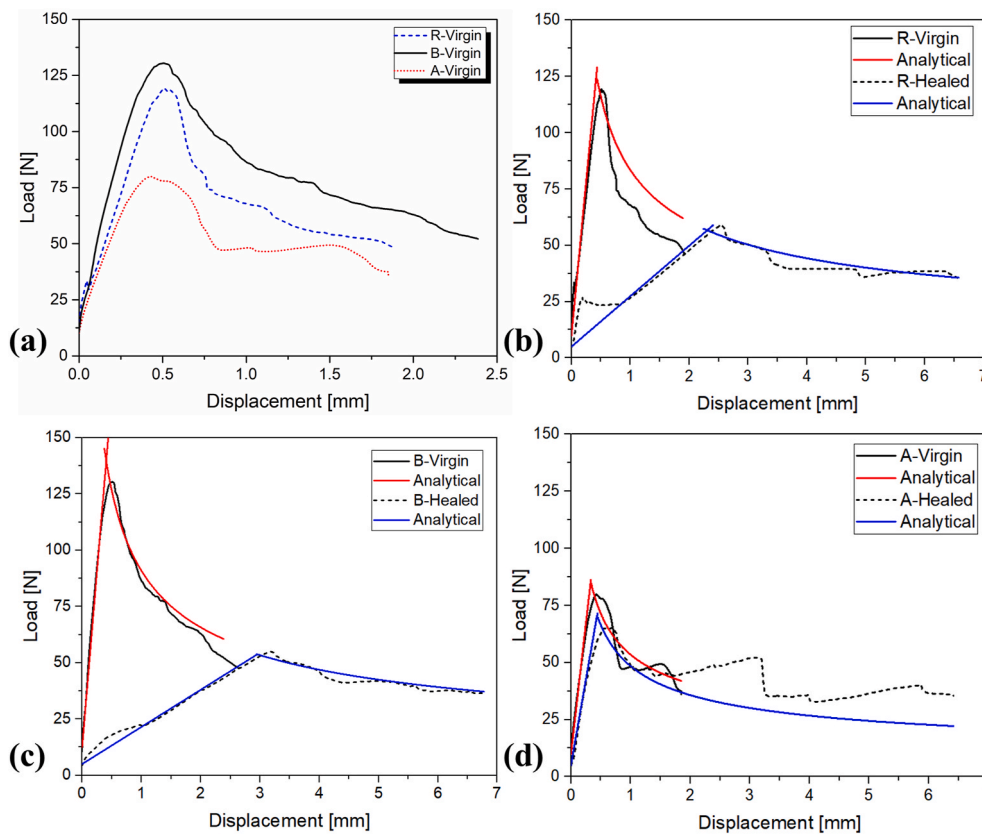
Fig. 9. The mode I load-displacement curve of a) virgin DCB specimens, b) virgin vs healed of adhesive R, c) virgin vs healed of adhesive B, and d) virgin vs healed of adhesive A.

described in section 3.4, and then they were subjected to the mode I test again with the same conditions of the virgin tests. The load-displacement curves of each healed specimen against its virgin state are depicted in Fig. 9b–d. Comparing the load-displacement curves of the healed specimens vs the virgin specimens revealed the fact that only the load curve of adhesive A followed the same trend as its virgin state, denoting its self-healing capability. The stiffness of the linear-elastic segment for both the virgin and healed adhesive A specimens was approximately the same (see Fig. 9d). This indicated the fact that the after-healing initial crack length was almost equivalent to the initial crack length (a_0) of the virgin case. When it comes to the other two adhesives (R and B), the response was different. In both cases, a significant reduction in the stiffness was observed suggesting that the after-healing initial crack length was different from the initial crack length in the virgin case. The values for the virgin and healed crack lengths are summarized in Table 2.

Due to the applied pressure and temperature during the healing process, some weak mechanical bonds were formed leading to an increase of the load as a function of the applied displacement up to ~20 N. Once these mechanical bonds were broken, the crack length reached the final/previous crack length (a) at which the virgin test was terminated. Starting from that point onwards, the load was correlated to the applied displacement again via the stiffness of the cantilever beam, but this time with a longer crack length (a). This was confirmed by the simple beam

theory (SBT) analytical load-displacement curves highlighted in red and blue for the virgin and the healed cases respectively (see Fig. 9b–d). The linear section of the curves was predicted using the SBT linear relationship between the applied displacement and the measured load as a function of the adherends' mechanical and geometrical properties. The propagation curves were calculated by equating the energy release rate with the average G_{IC} value of adhesives R, B and A, calculated by Equation (2). For the detailed derivation, the authors referred to the literature [45].

In order to create an index to quantify and compare the healing capability of each adhesive type, the energy as the area under the load-displacement curve for each case was utilized (see Fig. 10). The healing index in that sense was defined as the ratio between the energy dissipated via the healed specimens to reach the crack length at which the virgin test was terminated (a_V), denoted by E_H, and the energy dissipated during the virgin specimens testing to extend the crack from the initial crack length (a_{0-V}) to the final crack length (a_V), denoted by E_V (*Healing index* = E_H/E_V). If there was no healing, the loading curve of the healed specimen should follow exactly the unloading curve of the virgin case, thus the healing index should be zero. Based on the aforementioned explanation, the healing index for adhesives R, B and A was found to be 8.9%, 3.0%, and 82.5% respectively. Therefore, although adhesive A did not provide a high fracture toughness at its virgin state compared to the other two adhesives, it provided the highest healing capability amongst them.

The amplitude distribution of the AE signals originated during the mode I test of the virgin and healed DCB specimens is shown in Fig. 11. As depicted in Fig. 11a, c, and e, in the case of virgin specimens, significant AE events started a few moments after the start of the test, marked by a red circle on the x-axis. Few AE events that were observed in displacements less than the marked displacement could be due to the formation of some scattered micro-cracks around the manufacturing
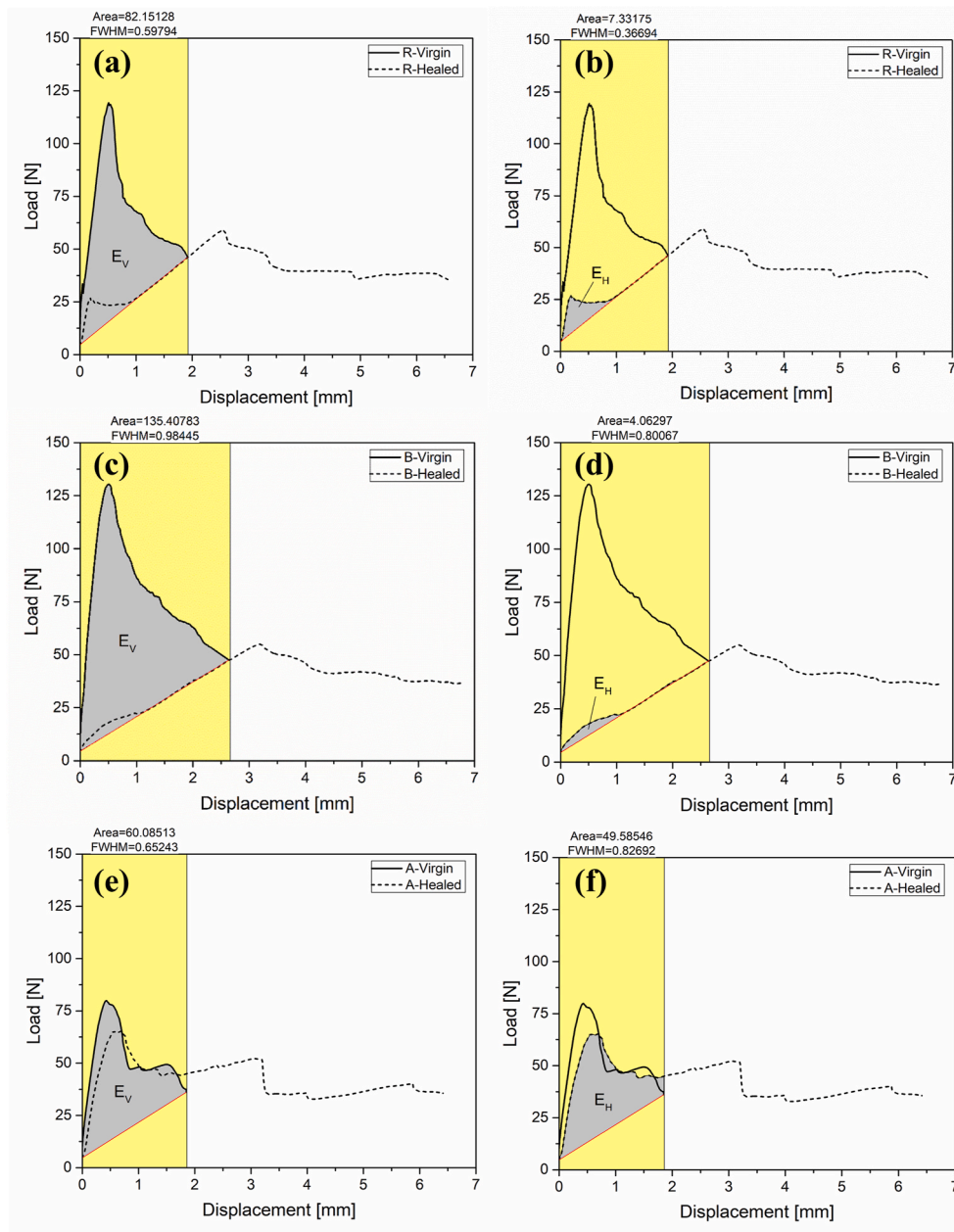
Table 2
The virgin and healed crack lengths in (mm) of one representative specimen.

	a_{0-V}	a_V	a_{0-H}
R	50	126	126
A	50	127	65
B	50	140	140

Fig. 10. Calculating the dissipated energy by the crack propagation in the virgin and healed DCB specimens; a) adhesive R-virgin, b) adhesive R-healed, c) adhesive B-virgin, d) adhesive B- healed, e) adhesive A-virgin, and e) adhesive A-healed.

imperfections within the adhesive layer, which can be neglected, because these micro-cracks do not result in significant fracture/failure. There was significant AE activity until the end of the virgin tests. Regarding the healed specimens, the AE events of adhesive A specimen started almost at the same displacement as its virgin state (see Fig. 11b). This indicated the high strength of the recovered bonds that almost experienced the same load of the virgin state, while in the case of adhesives B and R, the AE events of the healed specimens started earlier than of the virgin state that confirmed the formation of weak bonds in these adhesives (see Fig. 11d and f). From the AE point of view, the loading process of the healed B and R specimens can be divided into three regions: Region I, at which the weak bonds, which were formed during the healing process, carried small loads (~up to 20 N) before breaking. Region II, at which there was no new crack growth and there was just the elastic deformation of the aluminum cantilever beam arms. In this region, there was negligible AE activity. Region III, at which the

new crack propagates beyond a_V in the healed specimen, and a lot of new AE events were generated. However, in the case of adhesive A, there was no evidence of Region II in the loading process. In this case, the region I represented the breaking of the high-strength bonds formed during the healing process, followed directly by region III that was related to the formation and growth of the new crack beyond a_V in the healed specimen. The proposed AE segments were consistent with AE trends reported in the literature for the crack propagation in adhesively bonded joints [46].

As reported in the literature [47–49], the number of AE events that originated during the fracture of a healed material can be considered as an indication of the healing capability of the material, in the sense that the higher the AE activities, the higher the healing capability. In this context, the total number of AE events originated before the propagation of a new crack in the healed specimens (the total AE events of regions I and II for adhesives B and R, and the AE events of region I for adhesive A)
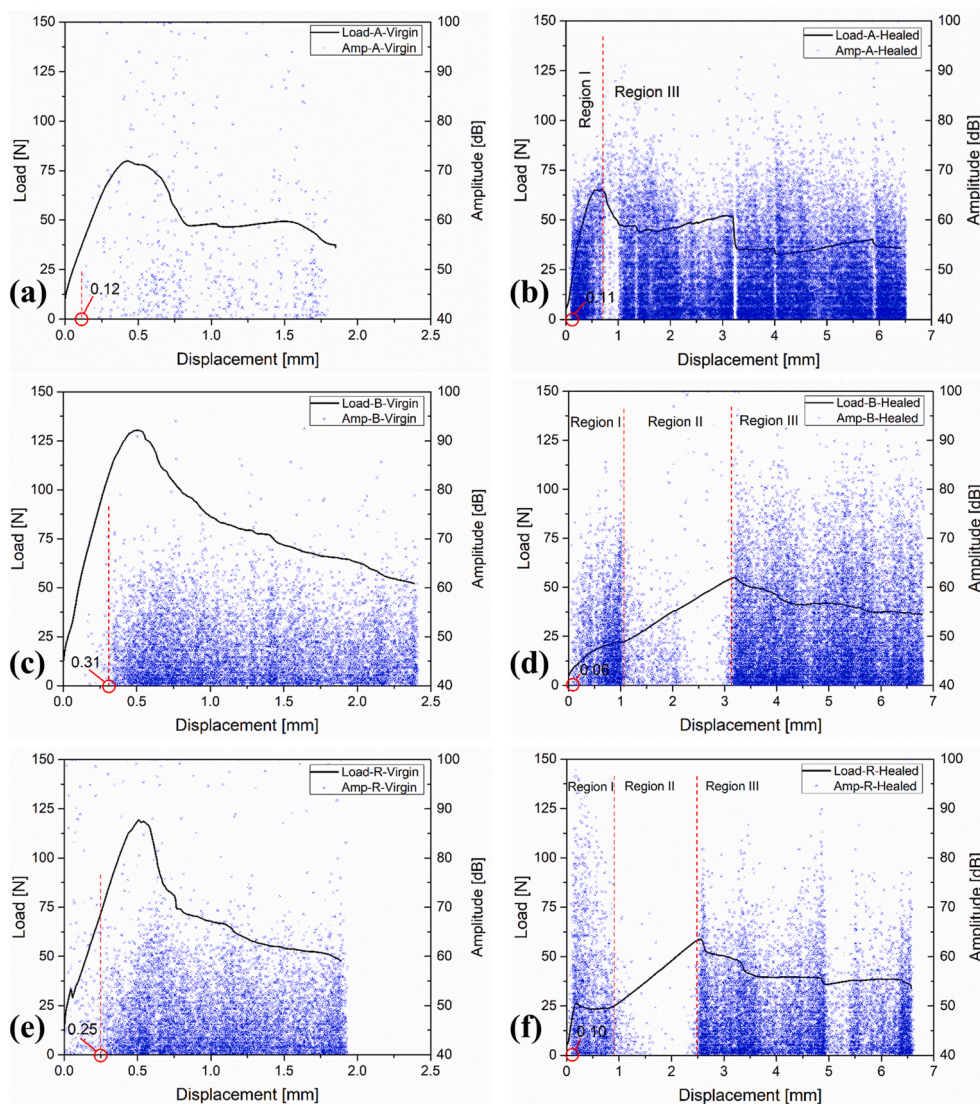
Fig. 11. Load-displacement curve and amplitude distribution of the AE signals recorded during the DCB tests; a) adhesive A-virgin, b) adhesive A-healed, c) adhesive B-virgin, d) adhesive B- healed, e) adhesive R-virgin, and e) adhesive R-healed.

was compared to the total number of AE events originated in the virgin tests. As it is depicted in Fig. 12c–f, there was a smaller number of AE activities at the end of the healing part for adhesives B and R compared to their virgin tests (4480 vs 10942 AE events for adhesive B, and 2510 vs 9825 AE events for adhesive R). This confirmed the low healing capability of these two adhesives. On the contrary, by comparing Fig. 12a and b, it was clear that the total number of AE events at the end of the healing part of adhesive A was much more than the total AE events of that adhesive in the virgin state (4360 vs 640 AE events). This increase in the AE events number after healing represented the breakage of additional mechanical bonds formed because of the high-applied pressure during the healing process moreover the high-strength recovered chemical bonds in adhesive A during the healing process. The same three regions stated in the case of AE amplitude can be observed here as well.

4.3. Fracture analysis

Post-mortem fractured surface of representative samples from each tested group after the self-healing process is presented in Fig. 13. The red line in Fig. 13 represents the initial crack length, which was the same for all tested samples (50 mm). Fig. 13a shows a complete adhesive failure of adhesive R with the adhesive on the lower adherend. This adhesive

also showed few defects in the bond-line, but since they were in the later testing stage, they didn't affect the presented results. In addition, the fractured surface of adhesive R showed the yellowing phenomenon caused by the formation of carbonyl groups on the DGEBA backbone as mentioned in section 4.1.2. The yellowing was noticed only in the fractured region (left) of the partially open specimen that was exposed to oxygen during the self-healing process (see Scheme 1). The uniform original brownish color was observed for adhesive A and B in Fig. 13 b and c, respectively, suggesting better thermal stability as confirmed by FTIR analysis in section 4.1.2. Fractured surfaces of adhesives A and B both showed adhesive failure with the crack transitions from one interface to the other. Nevertheless, the self-healing process didn't cause any observable structural changes or adhesive degradation for adhesive A and B, while the adhesive R requires additional stabilizers in its chemical formulation.

5. Conclusions

In this study, two eco-epoxide components based on TA were synthesized and utilized as a substitute for the BPA-based component: (A) glycidyl ether of TA and (B) glycidyl phosphate ester of TA. The effect of the modified TA component in a DGEBA epoxy formulation on the self-
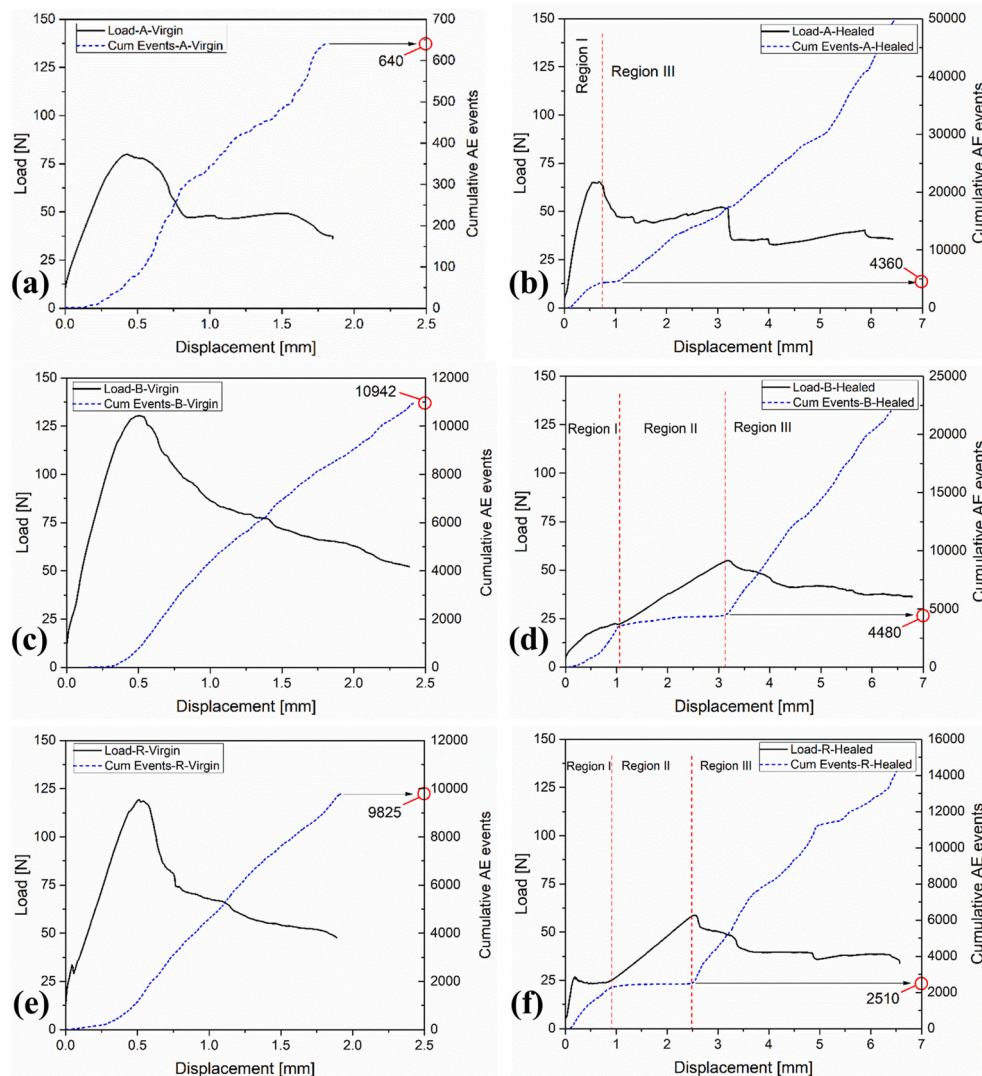
Fig. 12. The cumulative AE events curve for the three adhesives in the virgin and healed states; a) adhesive A-virgin, b) adhesive A-healed, c) adhesive B-virgin, d) adhesive B- healed, e) adhesive R-virgin, and e) adhesive R-healed.

healing of Al adherends was investigated. The residual activity and self-healing capability of adhesives were analyzed using DSC analysis, which revealed that adhesives exhibit residual reactivity at high temperatures and that adhesive A has a substantial healing capacity. After the high-temperature treatments, FTIR revealed structural alterations and suggested that R and A had the largest residual reactivity, indicating the possibility of self-healing. Additionally, the introduction of the modified TA improved thermal stability. DMA, on the other hand, demonstrated that adhesives A and B produced polymer networks with greater cross-linking density than adhesive R following the treatment. Finally, DCB testing was used to confirm the self-healing hypothesis. Only adhesive A specimens were able to regain substantial adhesion strength after the healing process. The healing index, defined by the energy dissipation ratio, for adhesives R, B and A was found to be 8.9%, 3.0%, and 82.5% respectively. Capturing AE events from the healed adhesive A specimens at the same point as the virgin samples indicated the high strength of the recovered bonds that almost withstood the same load of the virgin state. In the case of adhesives B and R, AE events of the healed specimens started earlier than their virgin counterparts, which confirmed the formation of weak bonds in these adhesives. After the self-healing process, a fracture analysis suggested that the self-healing treatment didn't affect adhesive A's structural integrity or cause any degradation, whereas the adhesives R and B had no self-healing potential. To summarize, the self-

healing theory of glycidyl ether of TA proposed in this work suggests that it has the potential to be used in adhesive formulations, with future research focusing on enhancing the adhesive characteristics of this bio-based component. The key aim in that regard would be to optimize the reactivity and steric hindrance of functional groups that have been added.

Author contributions

Conceptualization, N.Z.T., S.T.F., M.N.S., and M.S.; formal analysis, M.N.S., and M.S.; funding acquisition, N.Z.T., and S.T.F.; investigation, N.Z.T., M.N.S. and M.S.; methodology, M.N.S., S.T.F., and D.Z.; resources, A.M. and D.Z; software, M.N.S. and M.S.; supervision, S.T.F. and A.M.; validation, M.N.S., and S.T.F.; writing—original draft, N.Z.T., M. N.S., and M.S.; writing—review & editing, M.N.S., and S.T.F.

Data availability

The raw/processed data required to reproduce these findings cannot be shared at this time as the data also forms part of an ongoing study.
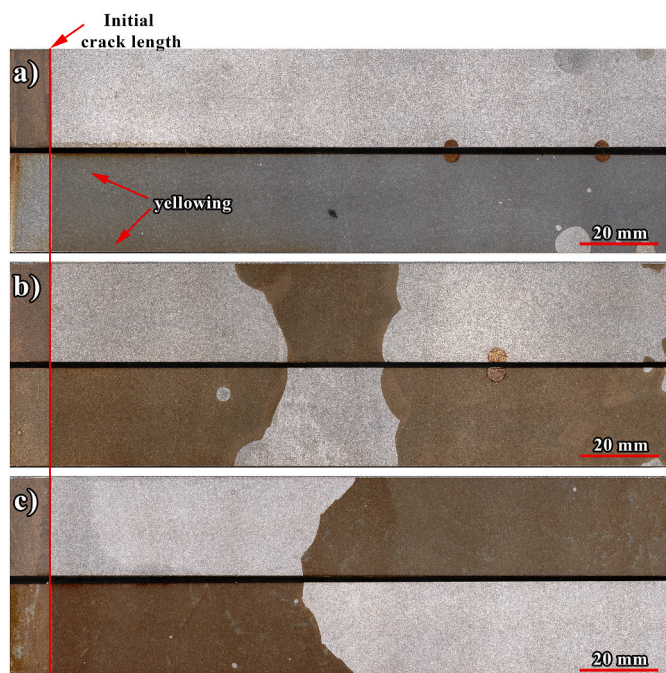
Fig. 13. Fractured surfaces of fully opened specimens after the self-healing process for adhesives: a) R, b) A, and c) B.

Declaration of competing interest

The authors declare that they have no known competing financial interests or personal relationships that could have appeared to influence the work reported in this paper.

Acknowledgment

References

[1] V.K. Thakur, M.K. Thakur, P. Raghavan, M.R. Kessler, Progress in green polymer composites from lignin for multifunctional applications: a review,, ACS Sustain. Chem. Eng. 2 (2014) 1072–1092, https://doi.org/10.1021/sc500087z.

[2] K. Jud, H.H. Kausch, J.G. Williams, Fracture mechanics studies of crack healing and welding of polymers, J. Mater. Sci. 16 (1981) 204–210, https://doi.org/10.1007/BF00552073.

[3] S. Varghese, A. Lele, R. Mashelkar, Metal-ion-mediated healing of gels, J. Polym. Sci. Part A Polym. Chem. 44 (2006) 666–670, https://doi.org/10.1002/pola.21177.

[4] Y. Yang, M.W. Urban, Self-healing polymeric materials, Chem. Soc. Rev. 42 (2013) 7446, https://doi.org/10.1039/c3cs60109a.

[5] Y. Yang, X. Ding, M.W. Urban, Chemical and physical aspects of self-healing materials, Prog, Polym. Sci. 49–50 (2015) 34–59, https://doi.org/10.1016/j.progpolymsci.2015.06.001.

[6] M. Kessler, N. Sottos, S. White, Self-healing structural composite materials, Compos. Part A Appl. Sci. Manuf 34 (2003) 743–753, https://doi.org/10.1016/S1359-835X(03)00138-6.

[7] M. Zhu, J. Liu, L. Gan, M. Long, Research progress in bio-based self-healing materials, Eur. Polym. J. 129 (2020) 109651, https://doi.org/10.1016/j.eurpolymj.2020.109651.

[8] S.R. White, N.R. Sottos, P.H. Geubelle, J.S. Moore, M.R. Kessler, S.R. Sriram, E. N. Brown, S. Viswanathan, Autonomic healing of polymer composites, Nature 409 (2001) 794–797, https://doi.org/10.1038/35057232.

[9] J.R. Kim, A.N. Netravali, Self-healing green composites based on soy protein and microfibrillated cellulose, Compos. Sci. Technol. 143 (2017) 22–30, https://doi.org/10.1016/j.compscitech.2017.02.030.

[10] S. Habib, A. Hassanein, R. Kahraman, E. Mahdi Ahmed, R.A. Shakoor, Self-healing behavior of epoxy-based double-layer nanocomposite coatings modified with Zirconia nanoparticles, Mater. Des. 207 (2021) 109839, https://doi.org/10.1016/j.matdes.2021.109839.

[11] L. Voorhaar, R. Hoogenboom, Supramolecular polymer networks: hydrogels and bulk materials, Chem. Soc. Rev. 45 (2016) 4013–4031, https://doi.org/10.1039/C6CS00130K.

[12] S.-H. Lee, S.-R. Shin, D.-S. Lee, Self-healing of cross-linked PU via dual-dynamic covalent bonds of a Schiff base from cystine and vanillin, Mater. Des. 172 (2019) 107774, https://doi.org/10.1016/j.matdes.2019.107774.

[13] R. Pugliese, F. Gelain, Characterization of elastic, thermo-responsive, self-healable supramolecular hydrogel made of self-assembly peptides and guar gum, Mater. Des. 186 (2020) 108370, https://doi.org/10.1016/j.matdes.2019.108370.

[14] J.K. Jethwa, A.J. Kinloch, The fatigue and durability behaviour of automotive adhesives. Part I: fracture mechanics tests,, J. Adhes. 61 (1997) 71–95, https://doi.org/10.1080/00218469708010517.

[15] L.J. Hart-Smith, A peel-type durability test coupon to assess interfaces in bonded, co-bonded, and co-cured composite structures, Int, J. Adhes 19 (1999) 181–191, https://doi.org/10.1016/S0143-7496(98)00033-5.

[16] H. Ghazali, L. Ye, M.-Q. Zhang, in: Lap Shear Strength and Healing Capability of Self-Healing Adhesive Containing Epoxy/mercaptan Microcapsules, 2016, p. 140004, https://doi.org/10.1063/1.4942339.

[17] H. Jin, G.M. Miller, S.J. Pety, A.S. Griffin, D.S. Stradley, D. Roach, N.R. Sottos, S. R. White, Fracture behavior of a self-healing, toughened epoxy adhesive, Int. J. Adhesion Adhes. 44 (2013) 157–165, https://doi.org/10.1016/j.ijadhadh.2013.02.015.

[18] S. Jahanshahi, A. Pizzi, A. Abdulkhani, A. Shakeri, Analysis and testing of bisphenol A—free bio-based tannin epoxy-acrylic adhesives, Polymers 8 (2016) 143, https://doi.org/10.3390/polym8040143.

[19] N.Z. Tomić, M.N. Saleh, S. Teixeira de Freitas, A. Živković, M. Vuksanović, J. A. Poulis, A. Marinković, Enhanced interface adhesion by novel eco-epoxy adhesives based on the modified tannic acid on Al and CFRP adherends, Polymers 12 (2020) 1541, https://doi.org/10.3390/polym12071541.

[20] Y.-O. Kim, J. Cho, H. Yeo, B.W. Lee, B.J. Moon, Y.-M. Ha, Y.R. Jo, Y.C. Jung, Flame retardant epoxy derived from tannic acid as biobased hardener, ACS Sustain. Chem. Eng. 7 (2019) 3858–3865, https://doi.org/10.1021/acssuschemeng.8b04851.

[21] ISO, 2009(en) - Adhesives — Determination of the mode 1 adhesive fracture energy of structural adhesive joints using double cantilever beam and tapered double cantilever beam specimens vol. 25217, 2009.

[22] M. Saeedifar, M.N. Saleh, S.T. De Freitas, D. Zarouchas, Damage characterization of adhesively-bonded Bi-material joints using acoustic emission, Compos. B Eng. 176 (2019) 107356, https://doi.org/10.1016/j.compositesb.2019.107356.

[23] M.N. Saleh, M. Saeedifar, D. Zarouchas, S.T. De Freitas, Stress analysis of double-lap bi-material joints bonded with thick adhesive, Int, J. Adhes. Adhes (2019) 102480, https://doi.org/10.1016/J.IJADHADH.2019.102480.

[24] B.R. Murray, S. Fonteyn, D. Carrella-Payan, K.-A. Kalteremidou, A. Cernescu, D. Van Hemelrijck, L. Pyl, Crack Tip Monitoring of Mode I and Mode II Delamination in CF/Epoxies under Static and Dynamic Loading Conditions Using Digital Image Correlation †, 2018, p. 5225, https://doi.org/10.3390/icem18-05225.

[25] F.X.Q.T. Hatakeyama, Thermal Analysis Fundamentals and Applications to Polymer Science Second Edition, John Wiley & Sons Ltd., West Sussex, 1999.

[26] N.Z. Tomić, A.D. Marinković, Đ. Veljović, K. Trifković, S. Lević, V. Radojević, R. Jančić Heinemann, A new approach to compatibilization study of EVA/PMMA polymer blend used as an optical fibers adhesive: mechanical, morphological and thermal properties, Int, J. Adhes. Adhes 81 (2018) 11–20, https://doi.org/10.1016/j.ijadhadh.2017.11.002.

[27] S. Doszlop, V. Vargha, F. Horkay, Reactions of epoxy with other functional groups and the arising sec-hydroxyl groups, Period. Polytech. - Chem. Eng. 22 (1978) 253–275.

[28] Z. Wu, S. Li, M. Liu, Z. Wang, X. Liu, Liquid oxygen compatible epoxy resin: modification and characterization, RSC Adv. 5 (2015) 11325–11333, https://doi.org/10.1039/C4RA14100H.

[29] F. Fraga, E.C. Vazquez, E. Rodríguez-Núñez, J.M. Martínez-Ageitos, Curing kinetics of the epoxy system diglycidyl ether of bisphenol A/isophoronediamine by Fourier transform infrared spectroscopy, Polym. Adv. Technol. 19 (2008) 1623–1628, https://doi.org/10.1002/pat.1178.

[30] O. Hara, Curing agents for epoxy resin, three bond tech, News (1990) 1–10.

[31] A. Krauklis, A. Echtermeyer, Mechanism of yellowing: carbonyl formation during hygrothermal aging in a common amine epoxy, Polymers 10 (2018) 1017, https://doi.org/10.3390/polym10091017.

[32] E. Ernault, E. Richaud, B. Fayolle, Thermal oxidation of epoxies: influence of diamine hardener, Polym. Degrad. Stabil. 134 (2016) 76–86, https://doi.org/10.1016/j.polymdegradstab.2016.09.030.

[33] Y. Zahra, F. Djouani, B. Fayolle, M. Kuntz, J. Verdu, Thermo-oxidative aging of epoxy coating systems, Prog. Org. Coating 77 (2014) 380–387, https://doi.org/10.1016/j.porgcoat.2013.10.011.

[34] K. Li, K. Wang, M. Zhan, W. Xu, The change of thermal–mechanical properties and chemical structure of ambient cured DGEBA/TEPA under accelerated thermo-oxidative aging, Polym. Degrad. Stabil. 98 (2013) 2340–2346, https://doi.org/10.1016/j.polymdegradstab.2013.08.014.

[35] E. Yousif, R. Haddad, Photodegradation and photostabilization of polymers, especially polystyrene: review, SpringerPlus 2 (2013) 398, https://doi.org/10.1186/2193-1801-2-398.

[36] D. Rosu, L. Rosu, C.N. Cascaval, IR-change and yellowing of polyurethane as a result of UV irradiation, Polym. Degrad. Stabil. 94 (2009) 591–596, https://doi.org/10.1016/j.polymdegradstab.2009.01.013.

[37] A. Živković, N. Tomić, M. Vuksanović, A. Marinković, Synthesis and characterization of epoxy resin coating with improved fire resistance by the addition of modified tannic acid, in: Proc. 8th Int. Conf. Renew. Electr. Power Sources, SMEITS, 2020, pp. 35–42, https://doi.org/10.24094/mkoiee.020.8.1.35.

[38] S. Zhao, M.M. Abu-Omar, Renewable epoxy networks derived from lignin-based monomers: effect of cross-linking density, ACS Sustain. Chem. Eng. 4 (2016) 6082–6089, https://doi.org/10.1021/acssuschemeng.6b01446.

[39] T.R. Crompton, Thermal Methods of Polymer Analysis, Smithers Rapra Technology Ltd, Shawbury, 2013.

[40] J.D. Menczel, R. Bruce Prime, Thermal Analysis of Polymers: Fundamentals and Applications, John Wiley & Sons, Inc., New Jersey, 2009.

[41] T. Kovačević, J. Rusmirović, N. Tomić, M. Marinović-Cincović, Ž. Kamberović, M. Tomić, A. Marinković, New composites based on waste PET and non-metallic fraction from waste printed circuit boards: mechanical and thermal properties, Compos. B Eng. 127 (2017) 1–14, https://doi.org/10.1016/j.compositesb.2017.06.020.

[42] A. Lavoratti, L.C. Scienza, A.J. Zattera, Dynamic-mechanical and thermomechanical properties of cellulose nanofiber/polyester resin composites, Carbohydr. Polym. 136 (2015) 955–963, https://doi.org/10.1016/j.carbpol.2015.10.008.

[43] M.N. Saleh, N.Z. Tomić, A. Marinković, S. Teixeira de Freitas, The effect of modified tannic acid (TA) eco-epoxy adhesives on mode I fracture toughness of bonded joints, Polym, Test 96 (2021) 107122, https://doi.org/10.1016/j.polymertesting.2021.107122.

[44] K. Mequanint, R. Sanderson, H. Pasch, Adhesion properties of phosphate- and siloxane-containing polyurethane dispersions to steel: an analysis of the metal-coating interface, J. Appl. Polym. Sci. 88 (2003) 900–907, https://doi.org/10.1002/app.11680.

[45] P.W. Harper, S.R. Hallett, Cohesive zone length in numerical simulations of composite delamination, Eng. Fract. Mech. 75 (2008) 4774–4792, https://doi.org/10.1016/j.engfracmech.2008.06.004.

[46] S. Teixeira de Freitas, D. Zarouchas, J.A. Poulis, The use of acoustic emission and composite peel tests to detect weak adhesion in composite structures,, J. Adhes. 94 (2018) 743–766, https://doi.org/10.1080/00218464.2017.1396975.

[47] Z. Jiang, Z. Yuan, W. Li, Acoustic emission analysis of characteristics of healing products in steam-cured cementitious materials with mineral additives, Construct. Build. Mater. 201 (2019) 807–817, https://doi.org/10.1016/j.conbuildmat.2018.12.140.

[48] K. Van Tittelboom, N. De Belie, F. Lehmann, C.U. Grosse, Acoustic emission analysis for the quantification of autonomous crack healing in concrete, Construct. Build. Mater. 28 (2012) 333–341, https://doi.org/10.1016/j.conbuildmat.2011.08.079.

[49] S. Granger, A. Loukili, G. Pijaudier-Cabot, G. Chanvillard, Experimental characterization of the self-healing of cracks in an ultra high performance cementitious material: mechanical tests and acoustic emission analysis, Cement Concr. Res. 37 (2007) 519–527, https://doi.org/10.1016/j.cemconres.2006.12.005.